The effect of Au nanoparticle spatial distribution on the stability of thin polymer films.

George Amarandei, [a] Colm O'Dwyer[b], Arousian Arshak[a], Uwe Thiele[c], Ullrich Steiner[d] and David Corcoran[a]*

[a] Department of Physics and Energy, University of Limerick, Ireland

[b] Department of Chemistry, University College Cork, Cork, Ireland and Tyndall National Institute, Lee Maltings, Cork, Ireland

[c] Department of Mathematical Sciences, Loughborough University, Loughborough, Leicestershire, LE11 3TU, UK

[d] Department of Physics, University of Cambridge, Cavendish Laboratory, JJ Thomson Avenue, Cambridge, CB3 0HE, UK

KEYWORDS. Gold nanoparticles, thin polymer film, stability, spinodal, dewetting

ABSTRACT. The stability of thin poly(methyl-methacrylate) (PMMA) films of low molecular weight on a solid substrate is controlled by the areal coverage of gold nanoparticles (NPs) present at the air-polymer interface. As the polymer becomes liquid the Au NPs are free to diffuse, coalesce and aggregate while the polymer film can change its morphology through viscous flow.

These processes lead at the same time to the formation of a fractal network of Au NPs and to the development of spinodal instabilities of the free surface of the polymer films. For thinner films a single wavelength is observed while for thicker films two wavelengths compete. With continued heating the aggregation process results in a decrease in coverage, the networks evolve into disordered particle assemblies while the polymer films flatten again. The disordering occurs first on the smallest scales and coincides (in thicker films) with the disappearance of the smaller wavelength. The subsequent disordering on larger scales causes the films to flatten.

1. Introduction

Thin films of hybrid materials, formed by mixing nanoparticles with polymer films [1–4] offer the possibility of creating materials with features on the nano/microscale with tunable properties due to nanoparticle-polymer, polymer-polymer and nanoparticle-nanoparticle interactions.[5,6] While there has been significant research on the stability of thin polymer films[7–12] and on particle aggregation,[13,14] the study of the stability of films of hybrid materials is still at an early stage.[15–17]

In Amarandei *et al.*[18] we describe the stability of thin polystyrene (PS) films covered by uniformly distributed Au nanoparticles (NPs). A PS film placed on a Si wafer (with a native oxide layer) is typically metastable, holes are nucleated and the film dewets.[7,9,10] We show that such films covered by Au nanoparticles are unstable, a spinodal instability develops, and that the stability is mainly influenced by the coverage of the films by nanoparticles. Moreover, a transition from unstable to stable films occurs when the Au coverage reduces through NP aggregation. As a result the polymer chain interconnections between neighboring particles are broken. As the PS chains tend to adhere to Au, the nanoparticles have a low mobility. Their aggregation occurs by a relatively slow coalescence process, involving the collision of migrating particles and subsequent recrystallization and reshaping into new nanoparticles, and/or Ostwald

ripening, in which diffusion of atoms through the polymer leads to the growth of larger particles at the expense of smaller ones.[13] Independently of the process, during their diffusion and aggregation on the thin polymer surface, the nanoparticles remain uniformly distributed.[18] As the coverage decreases, the van der Waals potential that controls the film stability becomes dominated by the thin polymer component, the system stabilizes and the film becomes flat again. We modeled the stability of a thin liquid PS film with the polymer-air interface uniformly covered by Au NPs and demonstrated that the well-known time evolution equation for the film thickness[7–12,18]

$$\partial_t h = -\nabla \cdot \left[\frac{h^3}{3\eta} \nabla \left(\gamma \Delta h - p_{\text{add}}(h) \right) \right] \qquad (1)$$

applies in the linear regime. Here, the pressure contains the Laplace (or curvature) pressure and the Derjaguin (or disjoining) pressure $p_{\text{add}} = \Pi = -\partial_h \Phi(h)$ where Φ is the wetting energy. For apolar materials Φ is a van der Waals potential that can be related to the dielectric properties of the various involved materials.[18] The film is linearly unstable for $\partial_{hh} \Phi(h) < 0$ with a fastest growing instability mode of wavelength $\lambda_{\text{m}} = \sqrt{-8\pi^2 \gamma / \partial_{hh} \Phi(h)}$.

Here we describe how the NP coverage and aggregation affect the stability of a NP-polymer film system in the case of NPs with high mobility, namely Au NPs on poly(methyl-methacrylate) (PMMA). The higher mobility of Au NPs on PMMA than on PS films[19] allows them to aggregate and coalesce. During their aggregation the NPs do not retain their initial uniform distribution and fractal networks form.[6, 20] The large mobility of the nanoparticles leads to cluster -cluster limited aggregation, and the fractal network is the signature of the particles' tendency to maximize the occupancy of available polymer surface.[21–23]

We present an experimental investigation into the stability of the thin films, and discuss the influence of different parameters on the stability. Thus, we show that the stability of a PMMA film that normally remains flat on a Si wafer covered by its native oxide changes because of the presence of the nanoparticles and their spatial distribution. We demonstrate that the Au NP network first forms and then disintegrates due to an aggregation and coalescence process. In response to the different phases the polymer film first develops a spinodal surface instability and then recovers the flat surface. Our investigation demonstrates that NP coverage may be used to tune the stability of a thin liquid polymer film.

2.Experimental details

Thin poly(methyl methacrylate) films [PMMA10, M_w = 10 kg/mol, R_g = 2.76 nm, M_w/M_n = 1.05, Sigma-Aldrich, UK] are obtained by spin coating from 2% (w/w) polymer solution in toluene onto Si wafers (and native oxide, $h_{SiOx} \simeq 2.0$ nm). Prior to spin coating the Si wafers with a resistivity of 2–3 Ω cm are cleaned in a jet of CO_2 ice crystals. Gold layers with nominal thicknesses of 1, 2, 2 and 3 nm are then sputtered at a low rate (0.09 nm s^{-1}) onto polymer thicknesses of 40, 39, 28 and 35 nm respectively creating in each case a Si/SiO_x/PMMA/Au NP/Air configuration.[18,24,25] On amorphous substrates such as polymer films, sputtering of metal can create metal islands that are free to diffuse and coalesce on the film surface. These nanometer objects are referred to in the present study as nanoparticles.[18,19,25] The Au deposition leads to uniformly distributed NPs on the polymer surface in the central region of the samples allowing a direct comparison between Si/SiO_x/PMMA/Air and Si/SiO_x/PMMA/AuNP/Air systems. Maintaining a constant deposition rate, the size of the nanoparticles is influenced only by the nominal thickness of the metal film. Thus, their size increases with the metal film thickness. A continuous Au film does not form for the nominal thicknesses of Au films deposited here (≤ 3

nm). The samples are heated at 170 °C, i.e. above the glass transition temperature of the polymer, and are removed and quenched at different time intervals.

Optical microscopy is employed to image surface morphology (**Figure 1** and **Figure S1**) and to acquire a non-contact optical profilometric measurement of surface roughness (**Figure 2b**) over large sample areas. Roughness, R, is the root mean square average of polymer height deviations and is calculated using

$$R = \sqrt{\sum_i \left(h_i - \bar{h}\right)^2 / N} \,,$$

where $\left(h_i - \bar{h}\right)$ is the local deviation of film height from the average value and N is the number of points where the height is measured. The measure of roughness presented in this work is the roughness value at each time step normalized to the mean value for all time steps. Optical imaging and roughness measurement are performed using a MicroPhase camera (PhaseView, France) placed on a Zeiss AxioImager A1.m microscope. The MicroPhase camera allows 3D visualization with highly repeatable non-contact optical surface profiling capabilities. For each time step a fast-Fourier-transform (FFT) of the optical images is performed, and the dominant wavelength is obtained (**Figure 1b** and **2a**). After Au deposition (at t = 0 min), no difference in roughness is measured between the central regions covered by Au NPs and the lateral regions that remain metal free.

Gold nanoparticle distributions are imaged using electron microscopy (**Figure 3**). The particle radius (R_p) and nearest neighbor center-to-center distance (d_{cc}) are acquired by image processing SEM images of the sample surface using SPIP (Image Metrology AS, Denmark) and the edge-to-edge distance between particles is calculated using $d_{ee} = d_{cc} - 2R_p$. The SPIP analysis at t = 0 min gives the initial distribution of particle radius sizes (**Figure S2**). R_p is the mean of the distribution (**Figure S3**) which increases with annealing time (**Figures S3** and **S4**). The SPIP

analysis allows the determination of the form shape factor S_f of the Au NPs and its variation with time (**Figure S5**). This reflects the relative circularity of the NPs and is given by $S_f = 4\pi A/P^2$, where A and P are the projected area and the perimeter of a NP as seen measured from SEM images. Thus, as S_f approaches 1, the projection of a NP resembles a circle.[13]

The box counting fractal dimension of the networks formed by the Au NPs imaged by SEM is measured using the Open Source image processing package FIJI, which is based on Image J (National Institutes of Health, USA). Only square images with the lateral length presented in **Figure 4** are used for the fractal dimension calculations. For illustration purpose, the full SEM images are presented to show large areas of the fractal networks (**Figure 3**, **S6** and **S7**).

3. Results

Figure 1 presents the time evolutions of the free surfaces of two thin polymer films (h = 28 nm left and h = 39 nm right), covered by Au NPs (h_{Au} = 2 nm). For the regions where the films are not covered by NPs (not shown in **Figure 1**), all films remain flat throughout the experiments. Locally, nucleation-triggered dewetting is sometimes observed, most probably caused by impurities (see **Figure S1** in the Supplementary Information). However, the nucleated holes do not grow and, therefore, the nucleation never leads to complete film rupture and drop bead-up. After 45 min of heating both films develop a spinodal pattern in the Au covered regions with similar surface topographies (**Figure 1**), and comparable instability wavelengths λ (**Figure 2a**) of 11 and 9 μm for the thinner and thicker film, respectively. In both films, λ increases up to the time t = 315 min (**Figure 2a**) revealing a power law $\lambda \sim t^{v}$ with values for v of 0.29 and 0.31, respectively.

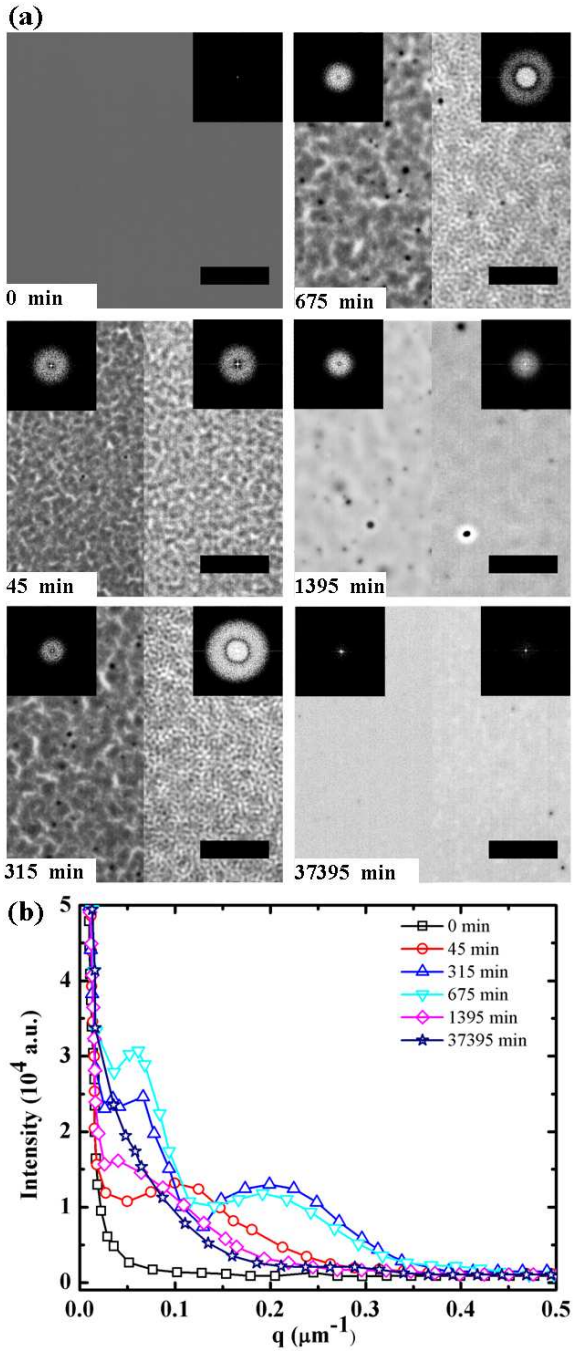

Figure 1. (a) Optical images of PMMA10 films covered by Au particles (h_{Au} = 2 nm), h_{PMMA10} = 28 nm (left) and h_{PMMA10} = 39 nm (right). The scale bars represent 50 μm. The insets are 2D FFTs of the images. (b) the radial averages of the FFT insets in (a).

Such a dependence of wavelength on time is commonly associated with a coarsening of the evolving structures.[10] Optically, the surface morphologies of the two polymer film surfaces (**Figure 1**) remain similar at t = 135 min (data not shown), although their topographies vary slightly due to the increasing instability wavelengths. As the instabilities develop the roughness in both films increases, and a maximum value is measured at t = 315 min (**Figure 2b**).

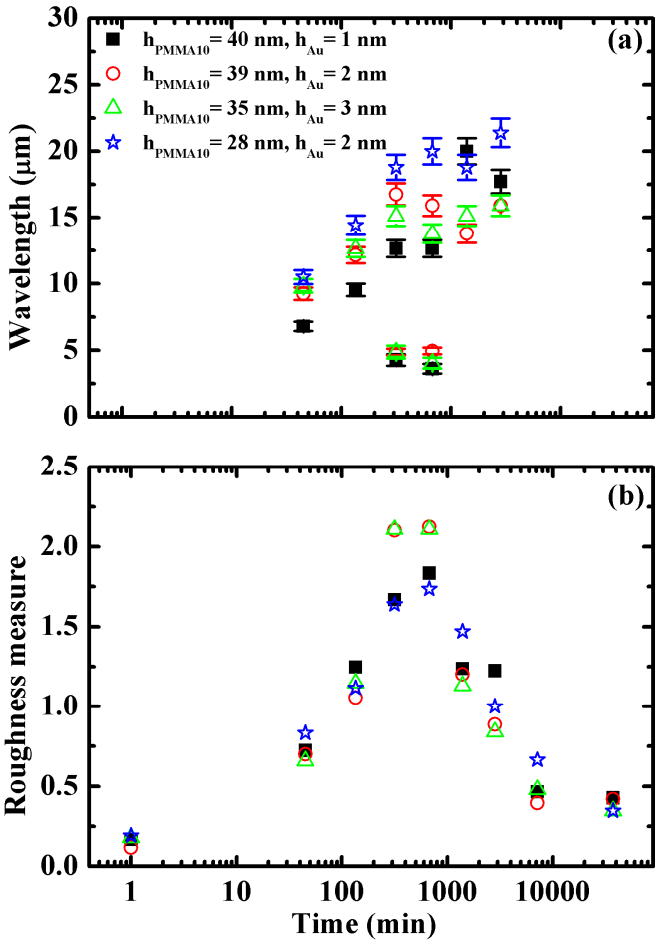

Figure 2. The time evolution of (a) wavelength and (b) roughness for PMMA10 polymer films covered by Au NPs.

Remarkably, in the next stage of the evolution the thicker film (h = 39 nm) develops fine wrinkle-like features as a second smaller wavelength appears between t = 315 min and t = 675 min (**Figures 1** and **2a**). No such features or smaller wavelengths are observed in the thinner film

(h = 28 nm). The roughness of both films attains a maximal value during this time (**Figure 2b**). The larger wavelength in the thicker film and the single wavelength in the thinner film saturate between t = 315 and t = 2835 min at comparable values (**Figure 2a**), the wavelength being slightly larger for the thinner film (λ ~ 20 μm). In the thicker films, the value of the smaller wavelength (λ ~ 5 μm) is approximately one-third of the corresponding larger wavelength (λ ~ 16 μm).

Continued heating leads in the final stage of the evolution to the disappearance of all features related to the smaller wavelength (**Figure 1** and **Figure 2a**) at t = 1395 min. The optical resemblance of the topographies of the two film surfaces is restored at this time (**Figure 1**) and the pattern amplitude in both films starts to diminish at t = 1395 min as reflected by the decrease in roughness (**Figure 2b**). At t = 7155 min the instabilities are completely suppressed and the films return to a flat state in which they remain during continued heating to 37395 min (**Figure 1**).

The existence of two wavelengths is confirmed for two other PMMA10 films of 40 and 35 nm in thickness, covered by Au layers with nominal thicknesses of 1 and 3 nm, respectively. For both samples, the first appearance of the initial spinodal instability, the appearance of the second smaller wavelength (again, ≈ 1/3 of the longer wavelength), and the disappearance of first the smaller and then the larger wavelength are observed at the same times as for the PMMA10 film with h = 39 nm covered by 2 nm of Au (**Figure 2a**). Fitting the wavelength increase for t < 315 min to $\lambda \sim t^{v}$ yields v = 0.32 and 0.21 for 1 and 3 nm thick Au layers, respectively. The trends in roughness for each sample are also remarkably alike (**Figure 2**). Note that at t = 1395 min the samples show a similar decrease in roughness that continues until the films become almost flat. These results suggest that the appearance of the second smaller wavelength is a characteristic of thicker films ($h \geq$ 35 nm) and is independent of the Au thickness.

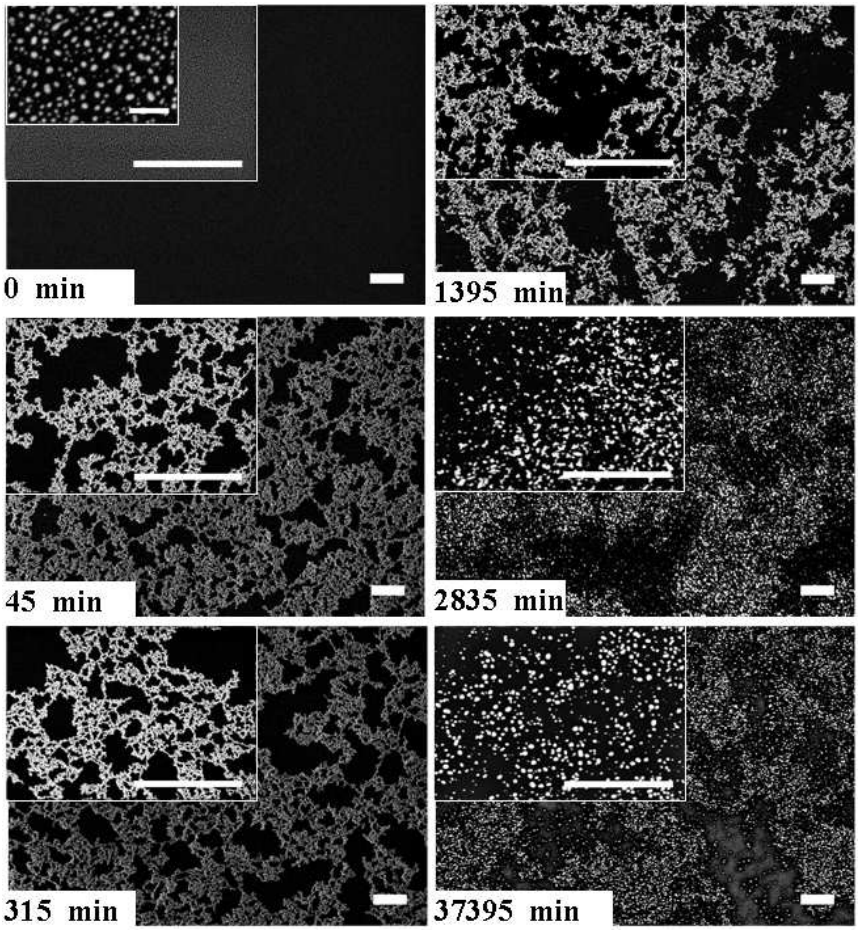

Figure 3. The Au nanoparticle distribution (nominal thickness h_{Au} = 2 nm) at different time steps for the h_{PMMA10} = 28 nm sample. The scale bars represent 1μm, with the exception of the smallest inset for t = 0 min where it represents 50 nm.

The distribution of the Au NPs is monitored by scanning electron microscopy (SEM) (**Figure 3**). For small nominal thicknesses of the Au layer, all the samples are, as previously seen for PS samples,[18] initially covered homogenously by Au nanoparticles of a certain size distribution (see the smallest inset at t = 0 min in **Figure 3** and **Figure S2**). The initial NP size is determined by the nominal thickness (as measured by the crystal monitor) of the deposited Au film. As seen in **Figure S2**, the mean particle radius increases with the thickness of deposited Au (**Figure S2** and also **S3**). Once the samples are heated, the polymer liquefies, the gold is free to move across the

film surface and the nanoparticles coalesce and aggregate. As a result, the mean radius of the nanoparticles grows with time (**Figures S3** and **S4**) as their size distribution shifts and broadens towards larger mean values of the radius (**Figure S4**). As the aggregation is due to a collision-coalescence process that is particle-migration-based,[13] the particles exhibit a relatively small form factor (**Figure S5**). The observed fluctuations in S_f (**Figure S5**), can be explained by the continuous reshaping of the particles.[13] At the time scales presented here, a competition occurs between the coalescence (that decreases the form factor) and surface energy which causes the aggregates to become spherical. The fluctuations of the form factor at intermediate times suggest that coalescence is the dominant process.[13]

As particles coalesce and aggregate, they do not retain the initial homogeneous coverage (**Figure 3** at t = 0 min) as seen in PS films where the NP mobility is low and the change in coverage is determined by Ostwald ripening or slow coalescence.[13,18] Instead, due to their higher mobility, at about t = 45 min the particles aggregate into a fractal network of *individual nanoparticles* (**Figures 3**, **S6** and **S7**), similar to the networks formed as a result of a cluster-cluster limited aggregation process.[20–23] At the same time, the film develops the spinodal instability discussed above (**Figure 1**).

The fractal network of Au NPs in the Au covered sample regions is similar regardless of where on a sample the SEM images are acquired, and the Au distributions on peaks and in troughs of the film surface are indistinguishable. The particle density is independent of surface topography. Au NP movement is dominated by Au-Au interactions which are several orders of magnitude larger than the Au-polymer interactions[19] and do not depend on the polymer film thickness. The particle movement and diffusion coefficient are controlled mainly by the particle size (i.e. their adhesion to the surface), liquid viscosity and particle density.

The changes that the Au NP spatial distribution undergoes in time are apparent in the SEM images for the thinnest polymer film sample (h = 28 nm, h_{Au} = 2 nm, **Figure 3**). From t = 45 to 675 min, the Au NPs exhibit a clear and well-defined fractal network. The network consists of regions with high particle densities and spaces devoid of particles on multiple scales (compare images with the insets at higher magnification for t = 45 min and t = 315 min in **Figure 3**). The regions of higher density are connected by narrow filaments of particles. In contrast, at 2835 min only a poorly defined remnant of the original fractal pattern is still visible. At smaller scales (see insets **Figure 3**) the network appears fragmented and the particle arrangement appears to be more homogeneous. This is even more pronounced at t = 37395 min (**Figure 3**) when the polymer surface is at a local scale again covered nearly homogenously by nanoparticles. The transition from the fractal to the disordered state is captured in the SEM image in **Figure 3** at t = 1395 min, where the fractal Au NP network appears to be breaking-up. While there are still regions of higher particle density in a fractal arrangement, the tenuous particle filaments between them are broken or in the process of disconnecting (for higher magnification see **Figure S6**).

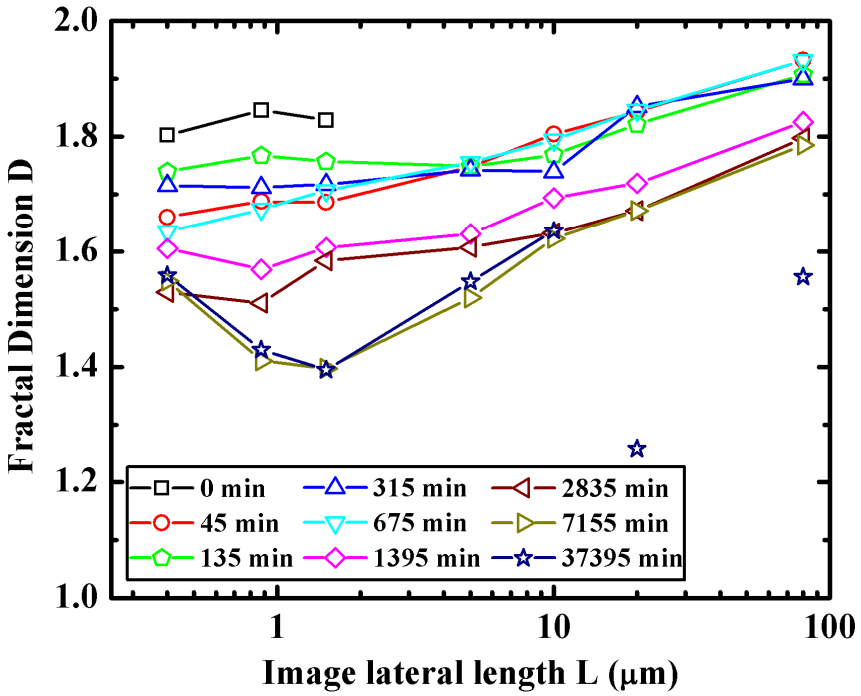

Figure 4. Fractal dimension of Au NP networks (h_{Au} = 2 nm) covering the h_{PMMA10} = 28 nm sample as a function of image lateral size *L*. The box-counting fractal dimension is calculated using bins of 2 to 64 pixels (1 nm ≤ 1 pixel ≤ 100 nm).

The arrangement of NPs can be characterized by calculating the box-counting fractal dimension *D* which is presented in **Figure 4** for the thinner PMMA film with h_{Au} = 2 nm. From *t* = 45 to 675 min at the smaller image scales (0.4 to 10 μm), the Au pattern has an approximately constant fractal dimension of *D* ~ 1.7 which is similar to gold colloidal aggregates in aqueous solution.[20] Above a characteristic length (ξ ~ 10 μm) the fractal dimension increases towards 2 suggesting that ξ is a correlation length,[26] corresponding here to the length scale of the largest open polymer spaces. At scales much greater than the correlation length, the Au distribution is expected to appear uniform. The fractal dimension at all scales below the correlation length corresponds directly to the well-defined Au NP fractal pattern observed in **Figure 3** (at *t* = 45 and 315 min, see also **Figure S6**).

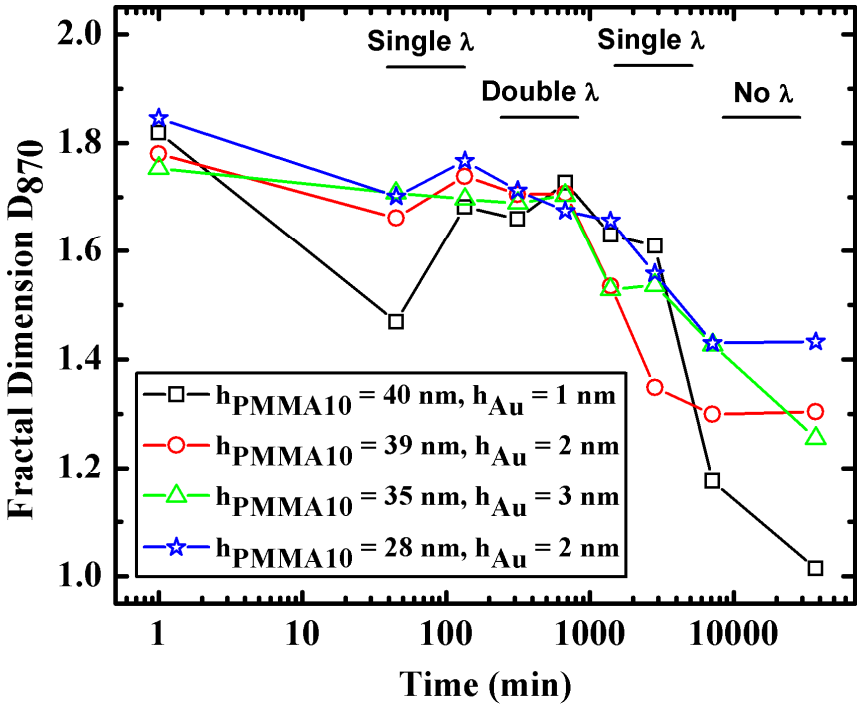

Figure 5. Fractal dimension of a square area of lateral size 870 nm for all PMMA10 samples. The presence of the wavelength(s) in the polymer films is indicated.

The transition to a more disordered network at t = 1395 min is reflected in the reduction of the fractal dimension to ~ 1.6 (on lateral scales of 0.4 to 5 µm), as the network starts to disintegrate, and the particle filaments break. A subsequent deterioration of the network is seen in D at t = 7155 to 37395 min when the fractal dimension reduces to ~ 1.4 on a lateral scale of ~ 1 µm.

At the larger scales (20 – 80 µm), SEM images reveal the Au to be distributed in a near uniform way although a fractal character is still apparent in an underlying 'coral-like' pattern which becomes more evident with heating time until in the final stages the Au particle arrangement appears to be homogeneous (**Figure S7**). The fractal dimension for the 80 µm lateral length image (**Figure 4**) remains constant from t = 45 to 675 min, dropping to ~ 1.8 from t = 1395 to 7155 min, and reducing again to ~ 1.6 at t = 37395 min.

Correlating the fractal analysis and SEM observations with the evolution of the surface instability, the following is revealed: The spinodal instability is present while the Au NP fractal network with D ~ 1.7 (0.4 to 10 μm) is seen; the disappearance of the second smaller wavelength mode occurs when the fractal dimension decreases to D ~ 1.6 (on a scale of 0.4 to 5 μm), as a consequence of network deterioration; the instability disappears entirely when the Au NP distribution is again nearly homogeneous and the fractal dimension is D ~ 1.4 on the ~ 1 μm scale. Given these correlations, it is likely that the Au NP arrangement has an effect on polymer film stability and may determine the appearance and form of the spinodal instability. Once the fractal network deteriorates to a homogeneous state, the Au NPs are no longer able to exert a collective effect on the polymer film and can influence it only locally at small length scales. The film behaves then as expected for a film with a homogeneous but low NP coverage[18] – the polymer film returns to a flat topography.

The time evolution of the Au NP fractal dimension at the image scale of 870 nm, where changes in D are most pronounced, is for all samples presented in **Figure 5**. The changes of D over time are broadly similar in all samples, regardless of polymer and Au film thicknesses. This supports the notion that Au-Au interactions dominate over the Au-PMMA interactions, and that the Au movement presented in **Figure 3** (see also **Figures S6** and **S7**) is not influenced by the topography of the polymer surface or the film thickness. In agreement with earlier observations, the disappearance of first the smaller and then the larger wavelength (related to the primary instability) corresponds to significant reductions in D, which indicates increased disorder and a deteriorating NP network. Interestingly, there is also a slight increase in the fractal dimension during the early development of the instability, and a modest decrease in D, as the second wavelength emerges.

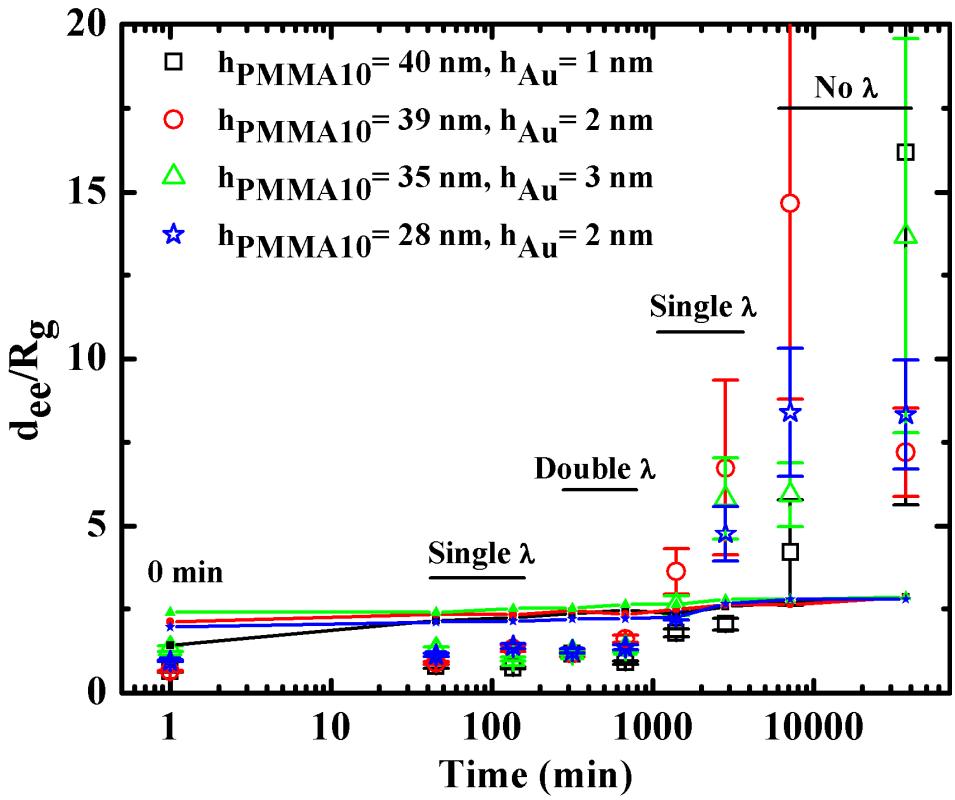

Figure 6. Mean edge-to-edge distance d_{ee} (large symbols) and connectivity limit d_m (small line-connected symbols) as function of time for all PMMA10 samples. The presence of the wavelength(s) in the polymer films is indicated.

As the particles diffuse and aggregate on the polymer surface, their number and size changes (**Figure S3**); as a result the distance between the NPs and the area of film covered by them also changes. Adapting for PMMA the model developed by Cole *et al.*[27] and following the procedure developed in Amarandei *et al.*[18] the maximal distance between two particles at which they are connected by polymer bridges can be established (small symbols in **Figure 6**). In this model, any polymer chain in contact with more than one NP at a time is defined as a ”bridge”. The total number of polymer chains ψ which have at least one segment in contact with a NP can be extracted as a function of the NP radius R_p and the polymer molecular weight M_w as $\psi_{PMMA} \cong 7.30R_p + 290M_w^{-1/2}R_p^2$. The average number of NPs which are bound together by

bridging molecules is given[18,27] by $\overline{N}_n = 2/\left(2-\varphi_c(d)\alpha\psi\right)$, where $\varphi_c(d)$ is the local volume fraction of contact chains, and α is the number of NPs at an inter-particle distance d that are available for bridging. Following Cole *et al.*[27] and taking $\alpha = 1$, the requirement that all NPs are connected by polymer i.e. $\overline{N}_n = \infty$ is $\varphi_c\psi = 2$. Using the experimentally determined mean radius of the NPs, ψ and φ_c, are calculated and the maximum edge-to-edge separation d_m for which NPs remain connected is extracted.[18,27]

The film stability can be then correlated with the presence of polymer bridges between NPs (**Figure 6**). As the particles aggregate, their coverage decreases, and therefore the distance between particles increases. The measured mean edge-to-edge distance d_{ee} between nearest-neighbor NPs is plotted versus time in **Figure 6** and compared with the theoretical bridging limit d_m.

Up to t = 675 min the mean edge-to-edge distance d_{ee} measured between nearest neighbors is smaller than the connectivity limit d_m while the spinodal instability is present (**Figure 6).** However, the films remain unstable even when d_{ee} becomes larger than d_m which is unlike the case of uniformly distributed NPs.[18] Note that for thicker films which exhibit two wavelengths, the smaller one disappears at this threshold for d_{ee}.

Although the spinodal instability persists for $d_{ee} > d_m$, we note that d_{ee} is the mean of a distribution of nearest neighbor distances and some particles may remain connected. Only when the fractal network has completely fallen apart, is the particle distribution sufficiently uniform *and* sparse so that $d_{ee} > d_m$ for all particles. At this point, the film returns to its flat state as seen at t = 7155 and 37395 min.

The aggregation process is slowed down by the bridges between the nanoparticles. These bridges cause the nanoparticles to move collectively and therefore have a lower diffusion

coefficient[27]. This effect is observed in the time dependence of the mean particle radius which does not increase significantly as long as the particles are connected (compare **Figure S3** and **Figure 6**). The NP spatial distribution does however change as reflected by the time evolution of the network fractal dimension (**Figure 4** and **5**). These changes in the network apparently lead to the changes in film stability.

A further factor that may retard the aggregation process is the particle size itself. The Stokes-Einstein diffusion equation of isolated spherical particles in a viscous medium[27] shows that the nanoparticle diffusion coefficient should decrease with increasing particle radius. This effect is expected to dominate in the late stages of the experiment when the particles are no longer connected by polymer bridges. Indeed, this explains the presence of the poorly defined remnants of the initial fractal pattern that remain visible at long times (e.g. t = 37395 min in **Figure S7**).

4. Discussion

The experimental results show that thin PMMA films covered by Au NPs heated above the glass transition temperature develop a spinodal instability, while bare regions remain flat. The stability of a bare polymer film on a coated solid substrate (here a Si wafer covered by a native SiO_x layer) is governed by effective molecular interactions between the air-polymer and polymer-substrate interfaces.[9] The different behavior of bare and NP-covered regions of the same polymer film implies that the presence of Au NPs at the polymer-air interface changes the interaction potential controlling the film stability.

Once the film is liquid, the particles are free to diffuse, coalesce and aggregate. During this process the NPs form an evolving fractal network. The polymer develops an initial spinodal instability as for homogeneously covered films (**Figure 7a**), followed for sufficiently thick films

by a second instability mode of smaller wavelength (**Figure 7b**). This secondary wavelength appears as wrinkles on the top of the first and later disappears.

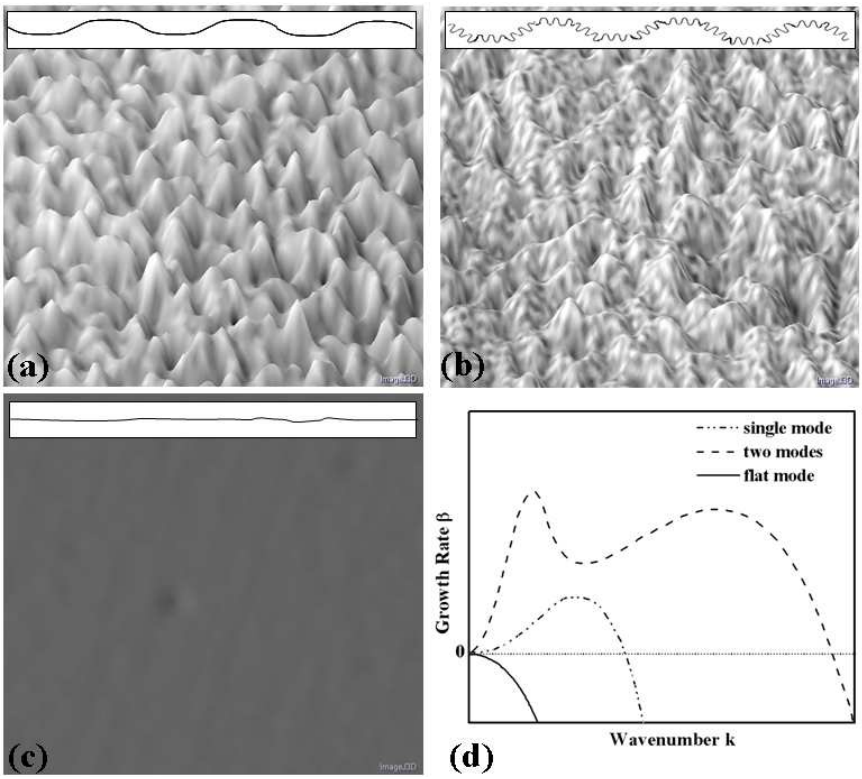

Figure 7. 3D representations of the optical micrographs of in **Figure 1** for (a) t = 135 min (single mode), (b) t = 315 min (two modes) and (c) t = 37395 min (flat mode). The schematic insets show the theoretical profiles of the surfaces. The differences between the wavelengths are exaggerated for illustration purposes. (d) An illustration of the dispersion relation i.e growth rate versus wavenumber for the different modes seen in the polymer films.

The evolution of these instabilities is related to the changing size and arrangement of the NPs, as characterized by the fractal dimension. With increasing NP aggregation, the Au coverage is reduced, the fractal network is eventually destroyed, and all surface instabilities disappear (**Figure 7c**). In other words, changes in the NP arrangement affect the interface potential that

determines the instability development. The way in which the fractal arrangement influences the instability appears to be linked to the polymer-connected NPs, as characterized by the edge-to-edge distance and its relationship to the connectivity limit, since there is a correlation between the breaking of this limit and the disappearence of the smaller of the two instability wavelengths.

For a thin film covered by NPs, the surface tension γ and the van der Waals potential Φ will depend on the fractional particle coverage $\Gamma(\vec{r},t) = A_p(t) \cdot \rho(\vec{r},t)$ where $A_p(t)$ and $\rho(\vec{r},t)$ are the mean cross-sectional particle area of the NPs and surface number density of NPs ($0 \le \Gamma(\vec{r},t) \le 1$ and $\vec{r} = x \cdot \hat{i} + y \cdot \hat{j}$).

The coverage-dependent surface tension is

$$\gamma(\Gamma) = \gamma(\vec{r},t) = \Gamma(\vec{r},t) \cdot \gamma_{AuNP} + (1 - \Gamma(\vec{r},t)) \cdot \gamma_{poly} \quad (2)$$

where, γ_{AuNP} and γ_{poly} are the Au nanoparticle surface tension (corrected for the variation with particle size A_p) and the bare polymer surface tension, respectively. In general, γ_{AuNP} in Equation 2 should be replaced by an interfacial energy γ_{interf} that may be approximated as a combination of polymer-nanoparticle and nanoparticle-air interfacial energies.[28] Here, as the materials involved are air, gold and polymer, this leads to $\gamma_{interf} \approx \gamma_{AuNP}$ as $\gamma_{AuNP} >> \gamma_{poly}$.

The total interaction potential is

$$\Phi(A_p, \Gamma, h) = (1 - \Gamma(\vec{r},t)) \cdot \Phi_{poly}(h) + \rho(\vec{r},t) \cdot \Phi_{AuNP}(h, A_p(t)) \quad (3)$$

where $\Phi_{poly}(h)$ is the effective interface potential of a thin polymer film on a SiO_x-covered Si substrate and $\Phi_{AuNP}(h,A_p)$ represents the van der Waals interaction between a single particle and a flat surface (see Suppl. Inf.).[18, 28]

For relatively immobile, uniformly distributed particles, their density, their mean size and therefore the film coverage are independent of position, i.e. $\rho(\vec{r},t) = \rho(t)$ and $\Gamma(\vec{r},t) = \Gamma(t)$. Using Equations (1) – (3), a linear analysis gives the condition for the stability of a NP-covered

film. This approach has been validated for Au-NPs on PS films.[18] Equations (1) - (3) may also be used to describe the nonlinear time evolution of the film.

For a thin film covered by mobile NPs, as in the present case of Au NPs on a PMMA film, the situation is more complicated as the system has more degrees of freedom. The particles are uniformly distributed on the film only at t = 0 and the system behavior is determined by the coupled evolution of the film thickness and particle coverage. In particular, the density $\rho(\vec{r},t)$ and coverage $\Gamma(\vec{r},t)$ vary in space and change in time in a complex manner. The behavior may be captured by coupled partial differential equations as discussed by Pototsky *et al.*[29,30] for two-layer films, Thiele[15] for films of mixtures and by Thiele *et al.*[31] for surfactant covered films. Such models allow one to explain coupling-induced instabilities and for some parameter regions, give rise to two competing instability modes, a behavior not covered by Equation (1). Although it is out of the scope of the current work to develop and analyze a detailed model for the present case, we will discuss its general form in analogy to Thiele *et al.*[31] and draw some general conclusions.

First we discuss the dependencies on material 'constants'. After linearization the surface tension (Equation (2)) is

$$\gamma(\Gamma) = \gamma(\vec{r},t) = \gamma(0) + \gamma_\Gamma \cdot \Gamma(\vec{r},t) \qquad (4)$$

where $\gamma(0) = \gamma_{\text{poly}}$ and $\gamma_\Gamma = \gamma_{\text{AuNP}} - \gamma_{\text{poly}} > 0$, in contrast to a surfactant on a liquid surface treated in Ref. 31 where $\gamma_\Gamma < 0$. Note that γ_{AuNP} slowly varies with time as the particles grow and coalesce. This results in a correction to γ_Γ. As a consequence of the existence of regions of higher and smaller NP density within the fractal networks observed here (**Figures 3**, **S6** and **S7**), the surface tension varies with position. Thus, in regions of high particle density (NP 'clusters') the surface tension (Equation (4)) is larger than in regions without particles ('voids'), where $\Gamma(\vec{r},t) = 0 \Rightarrow \gamma_{\text{void}} = \gamma_{\text{poly}}$. Regions of sparse NP density with particle filaments have

intermediate surface tensions. This implies $\gamma_{\text{cluster}} > \gamma_{\text{filament}} > \gamma_{\text{void}}$ as $\gamma_{\text{AuNP}} >> \gamma_{\text{poly}}$. The variation in surface tension also occurs on multiple length scales due to the fractal distribution of NPs and varies as the Au NPs coalesce and the NP distribution changes (**Figures 3** and **4**). The spatial variation of surface tension gives rise to tangential Marangoni forces at the free surface given by $\nabla_S \gamma = \gamma_\Gamma \nabla_S \Gamma$, where ∇_S is the derivative along the free surface. Changes in NP coverage are also expected to cause a spatial-temporal variation of the interaction potential Φ (Equation (3)).

It has recently been shown [Equation 23 in Ref. 31] that the evolution equations for a thin film covered by a surface active material that is insoluble in the bulk liquid are:

$$\partial_t h = \nabla \cdot \left[\frac{h^3}{3\eta} \nabla \left[\partial_h f(h,\Gamma) - \nabla \cdot (\gamma \nabla h) \right] - \frac{h^2}{2\eta} \left[\nabla \gamma - \Gamma \nabla \partial_\Gamma f(h,\Gamma) \right] \right] \tag{5a}$$

$$\partial_t \Gamma = \nabla \cdot \left[\frac{h^2 \Gamma}{2\eta} \nabla \left[\partial_h f(h,\Gamma) - \nabla \cdot (\gamma \nabla h) \right] - \left(\frac{h\Gamma}{\eta} + \tilde{D} \right) \left[\nabla \gamma - \Gamma \nabla \partial_\Gamma f(h,\Gamma) \right] \right] \tag{5b}$$

The surface active material may consist of surfactant molecules or surface-active nanoparticles. Which particular material these equations are applied to will affect the transport coefficients and energies but not the overall structure of the model. Thus we use the notion 'surfactant' for any surface active material. In Equations 5, $\tilde{D}$ is the diffusion coefficient and $f = f(\Gamma, h)$ is a general surfactant-dependent wetting energy and the surfactant-dependent γ results from entropic terms, surfactant-surfactant interactions, etc., as contained in the underlying free energy functional. Interpreting Γ as our particle coverage and *f* as our interaction potential *Φ* (given by Equation 3), the Equations 5 can describe the evolution of the PMMA film thickness and the Au NP surface coverage. Note that while the interactions characterizing the molecular surfactants differ from the interactions in the present NP system, these differences are reflected only in the particular

expressions for γ, Φ, η and $\tilde{D}$. Also, an attractive particle-particle interaction must be included in the energy functional to account for the observed particle aggregation into fractal networks.

For an imposed uniform particle distribution, i.e., without diffusion ($\tilde{D} = 0$), Equation 5a reduces to Equation 1 with the 1/3 in the mobility replaced by 1/12. Note that also disjoining pressure and surface tension in Equation 1 then depend parametrically on Γ. This applies to the case of Au NPs on thin PS films studied by Amarandei *et al.*[18] where the same particle density is measured in the instability peaks and troughs and the homogeneous coverage changes in time via coalescence.

Here for the Au NP-PMMA system, the condition for a spinodal instability $\partial_{hh}\Phi(h) < 0$ obtained from Equation 1, is also met at t = 0 min when the distribution of NPs is homogenous. All Au NP-PMMA systems studied lie initially above the spinodal line in a stability diagram (see **Figure S8**). As this is not changed by the additional degree of freedom (it does not make such a system more stable, cf. Ref. 30) these systems are expected to develop an initial instability, prior to NP coalescence taking place. However, the instability acts now on both fields and may initiate as well the growth of spatial variations in coverage whose development is faster for a larger diffusion coefficient.

A linear stability analysis of a system like our coupled Equations 5 can result in several types of dispersion relations that relate the growth rate of the instability to its wavelength (see sketches in **Figure 7d**). One may have[29,30]: (i) a single unstable dispersion curve corresponding to a single dominant growing wavelength (dot-dashed curve in **Figure 7d**), (ii) two individual unstable dispersion curves as the dot-dashed curve in **Figure 7d** corresponding to two growing wavelengths of which one is normally dominant, and (iii) a single unstable dispersion curve that has two maxima corresponding to two growing wavelengths (dashed curve in **Figure 7d**).

Although the stability of the system is purely determined by its free energy, the dominant instability modes, i.e., their wavelengths, growth rates and relative strengths of growth in the two fields depend strongly on transport parameters such as viscosity and diffusion coefficient. Indeed, it is possible that a change in the transport parameters alone may even change case (i) into case (iii) or vice versa.

Our knowledge about the involved material parameters and their dependencies on coverage, in particular, for the transport coefficients is not sufficient to actually solve Equations 5 for our system. The theoretical predictions can be tested by varying the polymer molecular weight. This changes the film viscosity and thereby the transport coefficients. The work here provides however generic knowledge about linear stability to interpret the complex experimental findings. For the thicker films we can distinguish 4 phases: (1) At t = 0 min the linear stability corresponds to case (i), a single wavelength develops (**Figure 7a**). As diffusion is sufficiently large, modulations develop in film height and coverage; (2) As the mean coverage changes the relevant dispersion curve is either of type (ii) or (iii) that both allow for two wavelengths to develop (**Figure 7b**). Note that the two modes do not need to involve film height and coverage in a similar way. In Ref. 29 the occurrence of the different modes was tuned by the films thickness, surface tension and viscosity ratios of the two layers. Here, the modes will be determined by the polymer film thickness and the particle coverage; (3) As the mean particle distance becomes larger than the bridging distance, first polymer bridges break, the transport coefficients and interaction terms change resulting again in a dispersion relation of type (i). Thereby, changes in the diffusion coefficient may reflect several effects: As the Au NP-Au NP interaction is much stronger than the Au NP – polymer interaction, it is primarily influenced by the aggregation process. Also, bridging connections between particles can change their effective diffusion coefficient, increasing the viscosity experienced by those particles collectively above the value of

the bulk polymer.[18,27] Thus, $\tilde{D}$ in Equation 5 is expected to be a function of $\rho(\vec{r},t)$ and consequently of $\Gamma(\vec{r},t)$; (4) Further coarsening changes the interaction potentials in a way that stabilizes the film (**Figure 7c**) as known from Au NP on PS.[18] In contrast to the thicker films (right images in **Figure 1**), the thinner films (left images in **Figure 1**) do not pass through phase (2), possibly because interaction potentials (and transport coefficients) differ and the type of dispersion curve depends sensitively on both.

In the present study, sputter deposition was chosen as it provides a spatially uniform NP distribution on polymer surfaces. The particle size, shape and coverage at $t = 0$ min are controlled by the deposition parameters, mainly the deposition rate and the nominal thickness of the deposited metal film. The particle size and their spatial distribution can be reproduced in a repeatable manner if the deposition parameters are unchanged.

Other techniques such as drop-casting, spin coating, dip-coating or spray coating are sometimes also used to deposit nanoparticles on polymer films. With these techniques, fractal-like structures often result immediately after NP deposition and those structures could cause the presence of lateral surface tension gradients from the outset, determining the magnitude of the Marangoni effect and its influence on the film stability. Importantly however, the general mathematical form of the theoretical model presented here remains valid.

In the above mentioned deposition methods, ligands normally cap the nanoparticles in order to avoid their clustering in solution. The interactions between the ligands and polymer matrix may have an influence on the composite polymer-nanoparticle instability as they affect not only their deposition and aggregation, but also their position on or within the polymer film. Ligands can for instance allow nanoparticles to embed into the liquid polymer film[3,4,6] forming a nanocomposite with different properties (viscosity, dielectric constant etc.). This, in turn, is characterized by a

different interaction potential Φ that controls the system stability. Moreover, after embedding the nanoparticles are still free to diffuse and aggregate. Under favourable conditions, the nanoparticles can segregate at the polymer-substrate interface, modifying the short-range interactions to overcome the long-range interactions.[18,32] The presence of ligands around the NPs can be included in in the interaction potential that controls the film stability. Such a potential must contain terms that capture the nanoparticle–ligand–polymer/substrate interactions.

In general, different deposition methods may lead to a more complex system compared to the films presented here. This additional complexity may exhibit a richer tableau of patterns that are interesting to study in the future.

Conclusions

We have shown that Au nanoparticle coverage is an important parameter in controlling the stability of thin liquid polymer films. Our results, obtained with PMMA films, have confirmed and extended results previously obtained with PS films. The development of spinodal surface instabilities shows stark differences that we have explained as resulting from the different mobility and adhesion of Au nanoparticles on PS and PMMA. Moreover, we have shown that the stability is independent of the particle distribution as long as the particles are interconnected by polymers. However, the wavelength of the spinodal surface instability is controlled by the particle distribution, which can result in a lateral variation in surface tension. For a sufficiently large variation in surface tension, a second smaller instability mode forms, driven by Marangoni and dispersion forces. This illustrates the possibility that two fast growing spinodal surface modes can develop at the same time, provided that the polymer film thickness is larger than some threshold.

AUTHOR INFORMATION

Corresponding Author

*George Amarandei, Department of Physics and Energy, University of Limerick, Ireland. Fax: +353 61 202423; Tel: +353 61 202625; E-mail: george.amarandei@ul.ie

Author Contributions

The manuscript was written through contributions of all authors. All authors have given approval to the final version of the manuscript.

ACKNOWLEDGMENT

We acknowledge support under EU Framework 7 for projects MRTN-CT-2004005728 (PATTERNS), PERG04-GA-2008-239426 (POLYPATT), PITN-GA-2008-214919 (MULTIFLOW) and from Tyndall National Institute through Science Foundation Ireland (SFI) funded National Access Programme (Project NAP 200). This work was also supported by SFI under contract no 07/SK/B1232a.

ASSOCIATED CONTENT

Supporting Information. Optical topography, and further information on nanoparticle size, shape and spatial distribution as described in detail in the main text, together with a phase diagram at t = 0 min and the detailed expression of the van der Waals potential interaction

between a nanoparticle and the underlying layers are included as additional material for this paper. This material is available free of charge via the Internet at http://pubs.acs.org.

REFERENCES

(1) Wong, H. C.; Cabral, J. T. Spinodal Clustering in Thin Films of Nanoparticle-Polymer Mixtures. *Phys. Rev. Lett.*, **2010**, *105*, 038301.

(2) Xavier, J. H.; Sharma, S.; Seo, Y. S.; Isseroff, R.; Koga, T.; White, H.; Ulman, A.; Shin, K.; Satija, S. K.; Sokolov, J.; Rafailovich, M. H. Effect of Nanoscopic Fillers on Dewetting Dynamics. *Macromolecules*, **2006**, *39*, 2972 – 2980.

(3) Jose-Yacaman, M.; Gutierrez – Wing, C.; Miki, M.; Yang, D. Q.; Piyakis, K. N.; Sacher, E. Surface Diffusion and Coalescence of Mobile Metal Nanoparticles. *J. Phys. Chem. B*, **2005**, *109*, 9703 – 9711.

(4) Deshmukh, R. D.; Composto, R. J. Direct Observation of Nanoparticle Embedding into the Surface of a Polymer Melt. *Langmuir*, **2007**, *23*, 13169 – 13173.

(5) Arceo, A.; Meli, L.; Green, P. F. Glass Transition of Polymer-Nanocrystal Thin Film Mixtures: Role of Entropically Directed Forces on Nanocrystal Distribution. *Nanoletters*, **2008**, *8*, 2271 – 2276.

(6) Meli, L.; Green, P. F. Aggregation and Coarsening of Ligand-Stabilized Gold Nanoparticles in Poly(methyl methacrylate) Thin Films. *ACS Nano*, **2008**, *2*, 1305 – 1312.

(7) Reiter, G. Dewetting of Thin Polymer-Films. *Phys. Rev. Lett*., **1992**, *68*, 75 – 78.

(8) Xie, R.; Karim, A.; Douglas, J. F.; Han, C. C.; Weiss. R. A. Spinodal Dewetting of Thin Polymer Films. *Phys. Rev. Lett*., **1998**, *81*, 1251 – 1254.

(9) Seemann, R.; Herminghaus, S.; Jacobs, K. Dewetting Patterns and Molecular Forces: A Reconciliation. *Phys. Rev. Lett*., **2001**, *86*, 5534 – 5537.

(10) Thiele, U. in *Thin Films of Soft Matter*, (ed. Kalliadasis, S. and Thiele, U.), Springer, Wien, 2007, Ch. Structure Formation in Thin Liquid Films.

(11) Baumchen, O.; Jacobs, K. Slip Effects in Polymer Thin Films. *J. Phys.: Condens. Matter*, **2010**, *22*, 033102.

(12) de Silva, J. P.; Geoghegan, M.; Higgins, A. M.; Krausch, G.; David, M. O.; Reiter, G. Switching Layer Stability in a Polymer Bilayer by Thickness Variation. *Phys. Rev. Lett.*, **2007**, *98*, 267802.

(13) Jia, X.; Listak, J.; Witherspoon, V.; Kalu, E. E.; Yang, X.; Bockstaller, M. R. Effect of Matrix Molecular Weight on the Coarsening Mechanism of Polymer-Grafted Gold Nanocrystals. *Langmuir*, **2010**, *26*, 12190 – 12197.

(14) Mukherjee, R.; Das, S.; Das, A.; Sharma, S. K.; Raychaudhuri A. K.; Sharma, A. Stability and Dewetting of Metal Nanoparticle Filled Thin Polymer Films: Control of Instability Length Scale and Dynamics. *ACS Nano*, 2010, **4**, 3709 – 3724.

(15) Thiele, U. Note on Thin Film Equations for Solutions and Suspensions. *Eur. Phys. J. Special Topics*, **2011**, *197*, 213 – 220.

(16) Clarke, N. Toward a Model for Pattern Formation in Ultrathin-Film Binary Mixtures. *Macromolecules*, **2005**, *38*, 6775 – 6778.

(17) Náraigh, L.Ó.; Thiffeault, J. L. Nonlinear Dynamics of Phase Separation in Thin Films. *Nonlinearity*, **2010**, *23*, 1559 – 1583.

(18) Amarandei, G.; O'Dwyer, C.; Arshak A.; Corcoran, D. The stability of thin polymer films as controlled by changes in uniformly sputtered gold. *Soft Matter*, **2013**, *9*, 2695 – 2702.

(19) Lopes, W. A. Nonequilibrium Self-assembly of Metals on Diblock Copolymer Templates. *Phys. Rev. E*, **2002**, *65*, 031606.

(20) Weitz, D. A.; Oliveria, M. Fractal Structures Formed by Kinetic Aggregation of Aqueous Gold Colloids. *Phys. Rev. Lett*., **1984**, *52*, 1433 – 1436.

(21) Haw, M. D.; Sievwright, M.; Poon W. C. K.; Pusey, P. N. Cluster-cluster gelation with finite bond energy. *Adv. Colloid. Interface Sci.*, **1995**, *62*, 1 – 16.

(22) Masschaele, K.; Fransaer J.; Vermant, J. Direct Visualization of Yielding in Model Two-dimensional Colloidal Gels Subjected to Shear Flow. *J. Rheol.*, **2009**, *53*, 1437 – 1460.

(23) Groot, R. D.; Stoyanov, S. D. Equation of State of Surface-Adsorbing Colloids. *Soft Matter*, **2010**, *6*, 1682 – 1692.

(24) Kunz, M. S.; Shull, K. R.; Kellock, A. J. Morphologies of Discontinuous Gold Films on Amorphous Polymer Substrates. *J. Appl. Phys.*, **1992**, *72*, 4458 – 4460.

(25) Smithson, R. L. W.; McClure, D. J.; Fennell Evans, D. Effects of Polymer Substrate Surface Energy on Nucleation and Growth of Evaporated Gold Films. *Thin Solid Films*, **1997**, *307*, 110 – 112.

(26) Stauffer, D.; Aharony, A. *Introduction to Percolation*, Taylor and Francis, London, 1994.

(27) Cole, D. H.; Shull, K. R.; Baldo P.; Rehn, L. Dynamic Properties of a Model Polymer/Metal Nanocomposite: Gold Particles in Poly(tert-butyl acrylate). *Macromolecules*, **1999**, *32*, 771 – 779.

(28) Israelachvili, J. N. *Intermolecular and Surface Forces*, Academic Press, U.K. 1992.

(29) Pototsky, A.; Bestehorn, M.; Merkt, D.; Thiele, U. Alternative Pathways of Dewetting for a Thin Liquid Two-layer Film. *Phys. Rev. E.*, **2004**, *70*, 025201.

(30) Pototsky, A.; Bestehorn, M.; Merkt, D.; Thiele, U. Morphology changes in the evolution of liquid two-layer films. *J. Chem. Phys.*, **2005**, *122*, 224711.

(31) Thiele, U.; Archer, A. J.; Plapp, M. Thermodynamically Consistent Description of the Hydrodynamics of Free Surfaces Covered by Insoluble Surfactants of High Concentration. *Phys. Fluids*, **2012**, *24*, 102107.

(32) Krishnan, R. S.; Mackay, M. E.; Duxbury, P. M.; Hawker, C. J.; Asokan, S.; Wong, M. S.; Goyette R.; Thiyagarajan, P. Improved polymer thin-film wetting behavior through nanoparticle segregation to interfaces. *J. Phys.: Condens. Matter*, **2007**, *19*, 356003.

BRIEFS.

The stability of thin liquid PMMA films is controlled by gold nanoparticles at the air-polymer interface. First, nanoparticles aggregate into fractal networks while spinodal surface instabilities develop. They show one and two wavelengths for thinner and thicker films, respectively. As the nanoparticle coverage decreases, the networks evolve into disordered particle assemblies while the polymer films flatten.

TOC Graphic

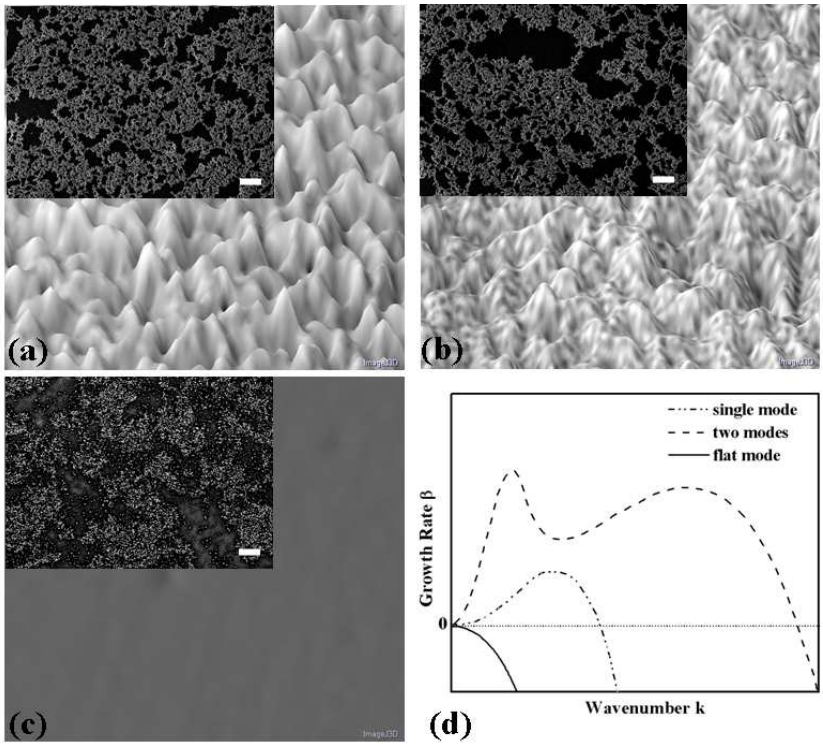

For Table of Contents only.